Chapter 4

Thermodynamic Description of the bcc Nb-Ti-V-Zr System

4.1 Introduction

The first aim of this work is to obtain a thermodynamic description of the bcc Nb-Ti-V-Zr system. As mentioned in Chapter 1, experimental phase diagram data are available for most of the binary systems. This data can be used for the thermodynamic assessment of the model parameters for the binary systems. Since such evaluations of the parameters ensure the reproducibility of the experimental data, we will obtain model parameters (CECs) for the binary systems directly from the thermodynamic assessment. This chapter gives details of the thermodynamic assessments of the binary phase diagram of Nb-Ti, Nb-V, Nb-Zr, Ti-V, Ti-Zr, and V-Zr systems. As mentioned previously, for the thermodynamic assessments, two types of data are used (i) phase diagram data and (ii) thermochemical data. Re-assessing these systems is desirable for two reasons: (i) to incorporate newly available thermochemical data based on first-principle calculations (details given in Chapter 3) and (ii) to model SRO in the solid solution phases. Details of optimization procedure in section 2.5 (Simultaneous optimization).

4.2 Nb-Ti System

The knowledge of the thermodynamic and phase diagram of the Nb-Ti system is very important in guiding the design and development of the Nb and Ti-based alloys. The equilibrium diagram of the system has been studied by Kaufman and Bernstain (1970), Murray (1981a), (J. L. Murray, Liao, and Spear 1987), Kumar et al. (K. C. H. Kumar, Wollants, and Delaey 1994), and Zhang et al. (Yuelan Zhang, Liu, and Jin 2001). The equilibrium phase diagram of the Nb-Ti system is simple and consists of three phases: liquid, bcc_A2(β), and hcp_A3(α). There is no invariant reaction. Murray reviews the

system in detail (Joanne L. Murray 1981a). The solidus boundary of the system was measured by Hansen et al. (1951), Rudy (1969), and Zakharov et al. (Zakharov, Pshokin, and Baikov 1969). There is no reliable data for the liquidus boundary. The solvus boundary showing the solubility of Nb in α-Ti (hcp_A3) was determined by Hansen et al. (1951), Imgram et al.(1960), Guzei et al. (Guzei, Sokoloyskaya, and Grigor'ev 1966), and Ronami et al.(1970). These points are in good agreement with each other. The β/(β+α) phase boundary data was obtained by Hansen et al. (1951), Imgram et al.(Imgram et al. 1960), Guzei et al. (Guzei, Sokoloyskaya, and Grigor'ev 1966), and Ronami et al.(1970) using metallography methods and in good agreement with each other. However, β/(β+α) boundary data of Brown et al. (1964) (Brown and Jepson 1966) was calculated using resistivity and lies considerably below the data obtained by metallography methods. Zhao et al. (J. Zhao and Notis 1993) proposed that the β/(β+α) boundary should be much higher than as assessed by Murray. Hence, data obtained using metallography methods were preferred by Zhang et al. (Yuelan Zhang, Liu, and Jin 2001). No reliable experimental thermodynamic data are available for the Nb-Ti system. Efforts have been made to obtain thermodynamic data using first-principle calculations (Raabe et al. 2007) (Marker et al. 2018). Chandran et al. (Chandran, Subramanian, and Gigliotti 2013) calculated the mixing enthalpy of body-centered cubic (BCC) β-Ti with transition elements using DFT-based first-principles methods. The SQS calculations for the Nb-Ti system performed by full relaxation did not significantly differ from the volume relaxed energies. Uesugi et al. (Uesugi, Miyamae, and Higashi 2013) reported that the enthalpies of the β phase decrease with increasing concentrations of Nb. Zhou et al. (W. Zhou, Sahara, and Tsuchiya 2017) reported similar results. Chinnappan et al. (Chinnappan, Panigrahi, and van de Walle 2016) have computed the sub-solidus equilibrium phase diagrams of Ti-Nb and other alloys through cluster expansion, lattice

dynamics, and Monte Carlo modeling methods combined with DFT total-energy calculations.

Simultaneous optimization

Simultaneous optimization has been done for the Nb-Ti system using the available experimental data from literature and the enthalpy of mixing data generated using first-principles calculations. The solidus data were taken from Rudy (1969), Zakharov (Zakharov, Pshokin, and Baikov 1969), and Hansen (1951). For β/α+ β and α /α+ β transus lines, data from Hansen (1951), Imgram (1960), and Ronami (1970) were taken. In the first step, parameters of the bcc_A2 phase were optimized with the help of the enthalpy of mixing data generated using first-principles calculations. Next, parameters of the liquid phase were optimized using solidus data, followed by the hcp_A3 phase using β/α+ β and α /α+ β boundaries data. Lastly, the parameters of all phases were optimized further with the help of the entire dataset. Efforts were made to keep the number of parameters minimum. The optimized parameters are given in

Table 4-1. A good description of the Gibbs energy for the bcc and hcp phases was obtained using parameters related to the first and second neighbor pairs only. The second neighbor pair CEC for the bcc phase is fixed as 2/3rd of the first neighbor CEC in these assessments since independent optimization of these parameters often leads to non-physical values. Temperature dependence of all the parameters was not needed to fit experimental data. Due to the different modeling approaches used, the model parameters for the bcc phase cannot be compared with those found earlier. The calculated phase diagram is shown in Figure 4-1. A comparison with the numerous experimental data on the solidus and liquidus is given in Figure 4-2, and a reasonably good agreement may be seen. Figure 4-3 shows the calculated α/β boundaries and experimental information. Reasonable compliance between them may be observed. Calculated thermodynamic data

is compared with the enthalpy of mixing data generated using first-principles calculations in Figure 4-4. Deviations from the first-principles calculations may be observed near the Ti end since more weightage is given to the experimental data while optimizing the parameters in this work.

Table 4-1 Optimized set of CECs used in assessing the Nb-Ti phase diagram.

Phase	Parameters (J/mol)
bcc_A2 phase	$C_2^{\beta} = 335 + 0.088213 * T$ (I-neighbor pair)
	$C_3^{\beta} = 223.33 + 0.0588087 * T$ (II-neighbor pair)
hcp_A3	$C_2^{\alpha} = 426$ (I-neighbor pair)
	$C_3^{\alpha} = 426$ (II-neighbor pair)
Liquid	L_0^{l} =-19150

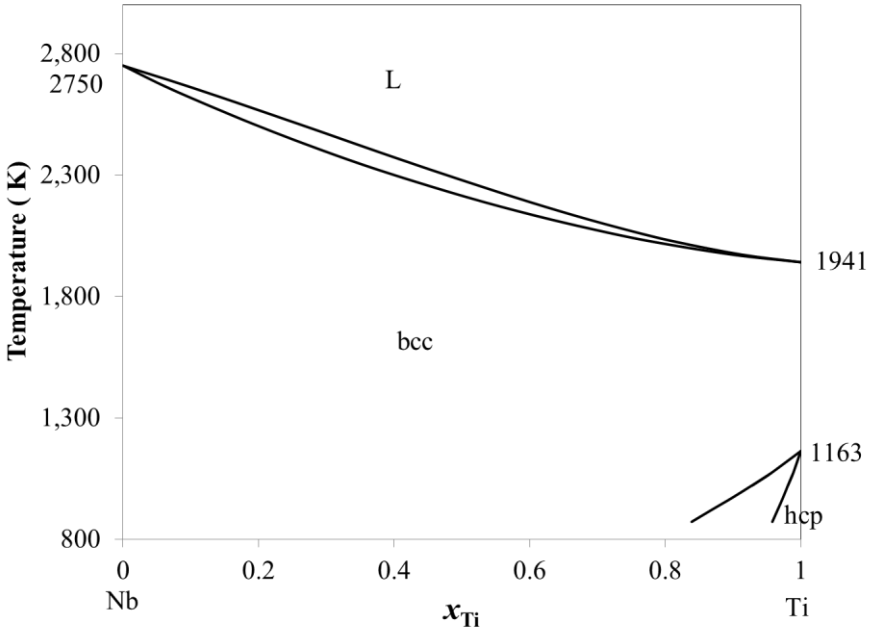

Figure 4-1 Calculated phase diagram of the Nb-Ti system

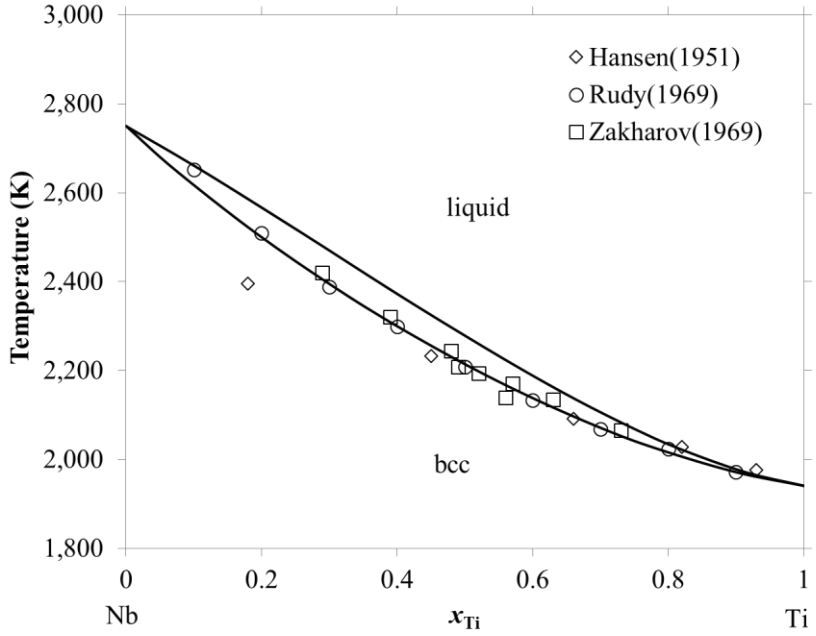

Figure 4-2 Calculated liquidus and solidus boundaries in the Nb-Ti system and experimental solidus data (Rudy (1969), Zakharov (Zakharov, Pshokin, and Baikov 1969), and Hansen (1951)).

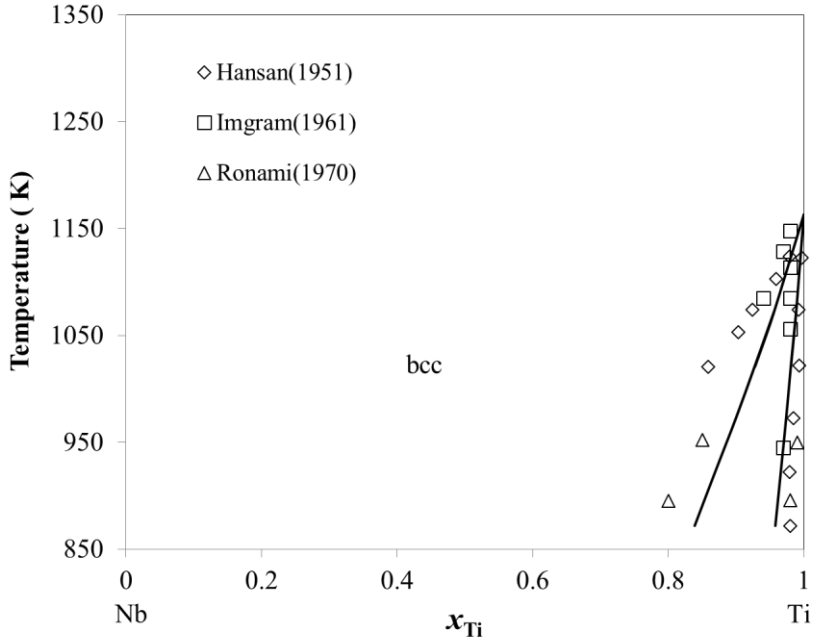

Figure 4-3 Calculated α/β boundary of the Nb-Ti System and experimental data.

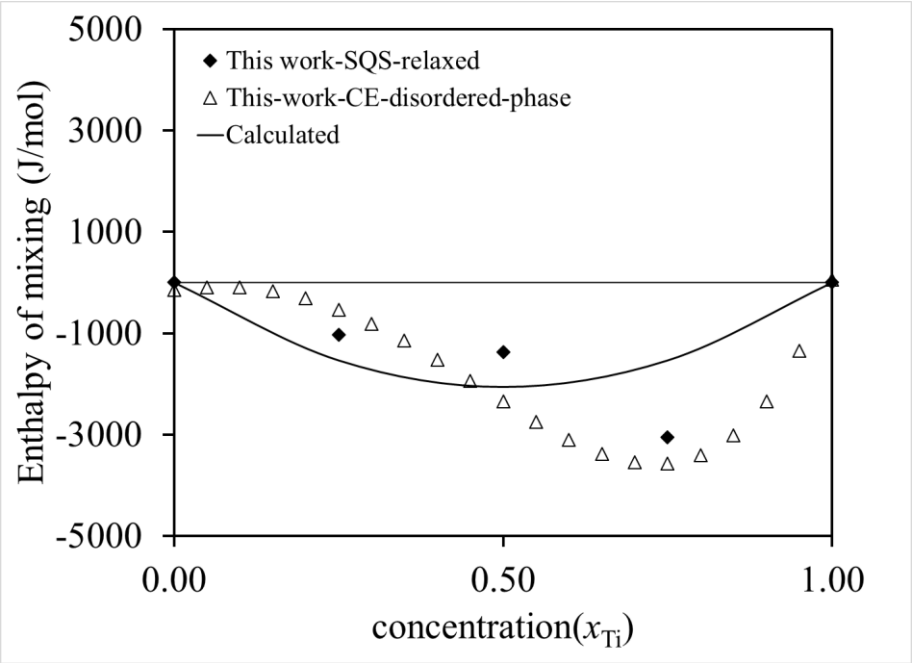

Figure 4-4 Calculated enthalpy of mixing of the Nb-Ti bcc phase at 1900 K (solid line) along with calculated data in this work.

4.3 Ti-V system

The binary Ti-V system is a simple system with no intermediate phase. The equilibrium phases of the Ti-V system are liquid, hcp_A3(α), and bcc_A2(β) solid solution phases. Ti-V System was reviewed by Murray (1981b) in 1981. Solidus data was reported by Adenstedt *et al*. (Adenstedt, Pequignot, and Raymer 1952) and Rudy (1969). Rudy's (1969) data is considered more accurate. For the α/(α+β) boundary, data from Adenstedt *et al*. (Adenstedt, Pequignot, and Raymer 1952) and Molokanov (Molokanov, Chernov, and Budberg 1977) is available. Similarly, Adenstedt *et al*. (Adenstedt, Pequignot, and Raymer 1952) and Ermanis (Ermanis, Farrar, and Margolin 1961) have reported data for the (α+β)/β boundary.

Experimental thermodynamic data for this system is very limited. Jain et al. (Jain, Mukherjee, and Dey 2016) have reported the activity of V-4Ti alloy. Skripnyak *et al.*

(2020) experimentally measured the mixing enthalpy of bcc Ti-V alloys at 1073 K and found enthalpies to be positive. DFT-based FP methods based were used to calculate thermodynamic data for this system by various researchers (Chandran, Subramanian, and Gigliotti 2013) (Uesugi, Miyamae, and Higashi 2013) (Chinnappan, Panigrahi, and van de Walle 2016)(Skripnyak et al. 2020). The Ti–V system was optimized by Murray (Joanne L. Murray 1981b), Saunders (Saunders 1998), and Ghosh (Ghosh 2002)

Simultaneous optimization

The solidus data were taken from Rudy (1969). For α/β boundaries, data from Adenstedt *et al*. (Adenstedt, Pequignot, and Raymer 1952), Ermanis (Ermanis, Farrar, and Margolin 1961), and Molokanov (Molokanov, Chernov, and Budberg 1977) were used. Enthalpy of mixing data given by Skripnyak et al. (2020) was also considered to optimize the parameters. In the first step, parameters of the bcc_A2 phase were optimized with the help of the experimental enthalpy of mixing data. Next, parameters of the liquid phase were optimized using solidus data, followed by the hcp_A3 phase using α/β boundaries data. Lastly, the parameters of all phases are refined further with the help of the entire dataset.

The optimized parameters are given in Table 4-2. Temperature dependence of all the parameters was not needed to fit experimental data. The calculated phase diagram is shown in Figure 4-5. A comparison with the numerous experimental data on the solidus and liquidus is given in Table 4-6 and a reasonably good agreement may be seen. Figure 4-7 shows the calculated α/β boundaries along with experimental information. Good compliance between them may be observed. Calculated thermodynamic data compare well with the experimental enthalpy of mixing data generated using first-principles calculations (Figure 4-8).

Table 4-2 Optimized set of CECs for assessing the Ti-V phase diagram.

Phase	Parameters (J/mol)
bcc_A2 phase	$C_2^{\beta} = -496 + 0.092 * T$ (I-neighbor pair)
	$C_3^{\beta} = -330.67 + 0.06133 * T$ (II-neighbor pair)
	$C_4^{\beta} = -12.142$ (triangle)
hcp_A3	$C_2^{\alpha} = -567.63$(I-neighbor pair)
	$C_3^{\alpha} = -567.633$ (II-neighbor pair)
Liquid	$L_0^l = 1400.000$ $L_1^l = -1341.677$

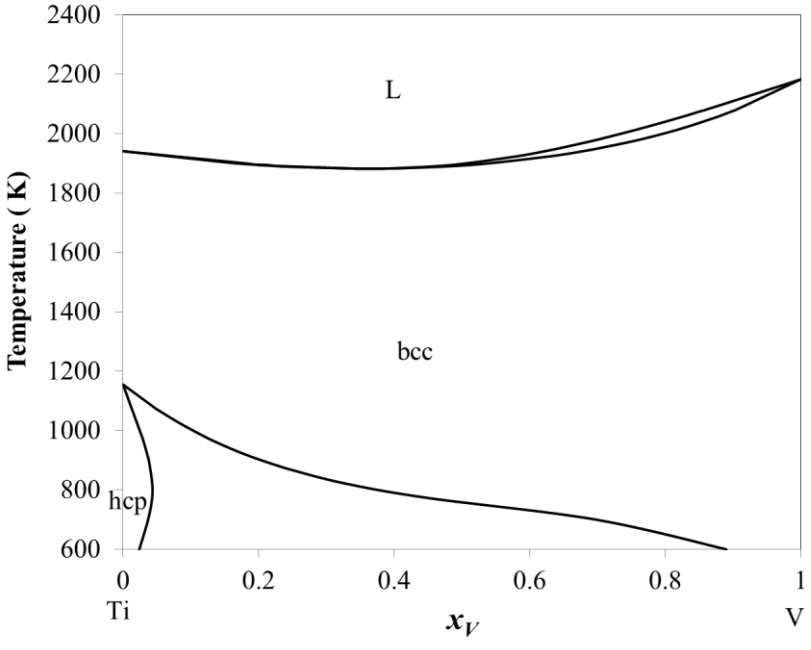

Figure 4-5 Calculated phase diagram of the Ti-V system

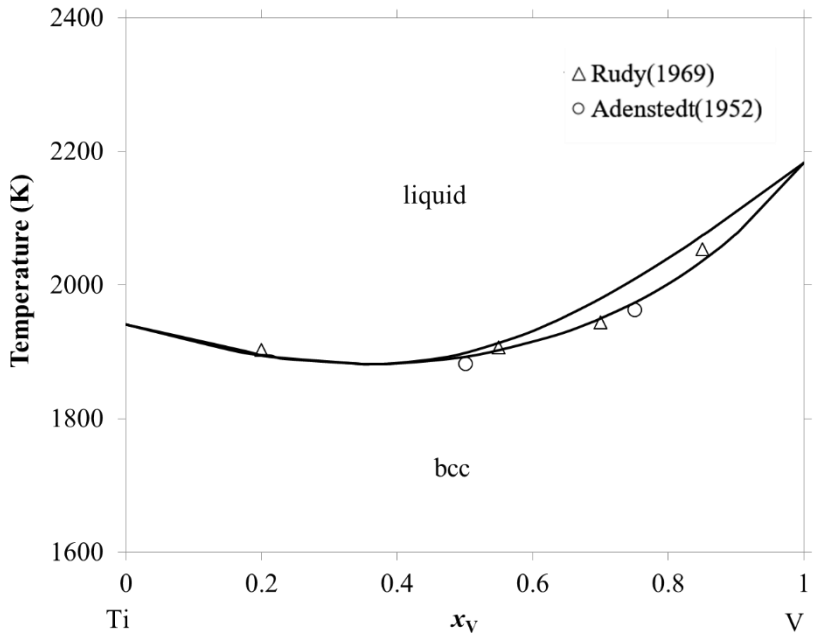

Figure 4-6 Calculated liquidus and solidus boundaries in the Ti-V system and experimental data.

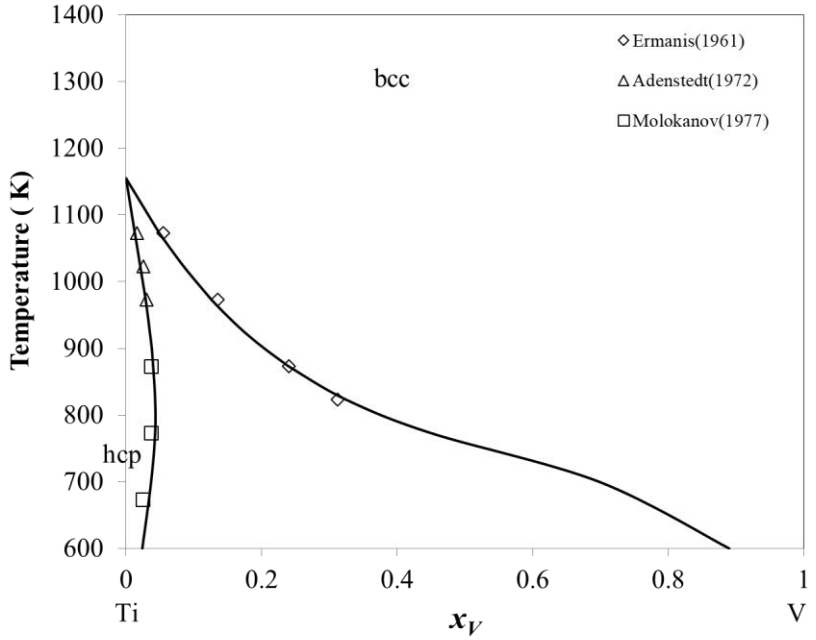

Figure 4-7 Calculated α/β boundary of the Ti-V System and experimental data.

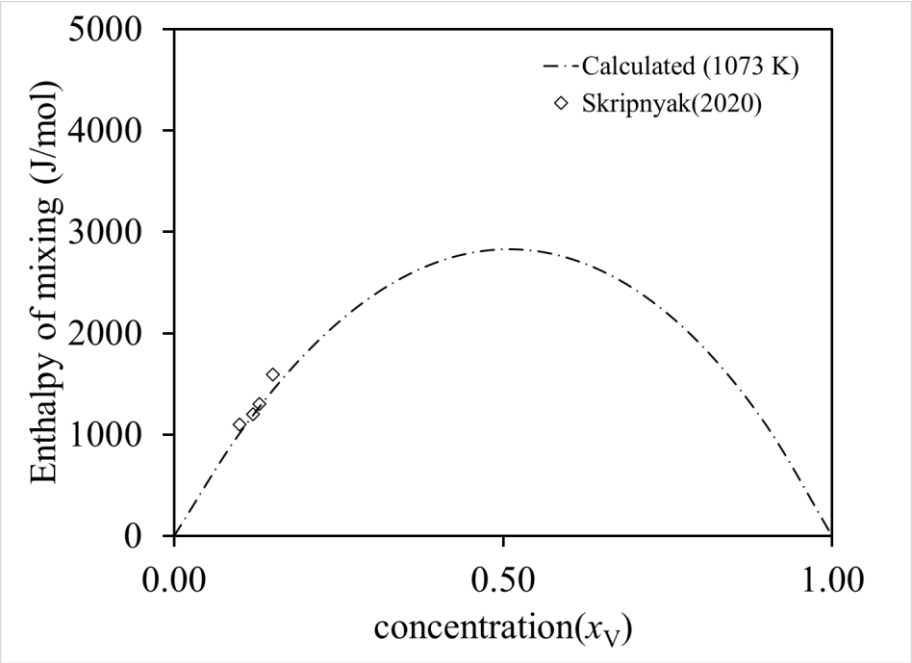

Figure 4-8 Calculated enthalpy of mixing of the bcc phase at 1073K (solid line) along with experimental data of Skripnyak et al. (2020) for Ti-V system.

4.4 Ti-Zr system

The phase diagram of Ti-Zr consists of three phases liquid, hcp_A3(α), and bcc_A2(β), and shows complete liquid and solid solubility. There are two congruent transformations: (i) Liquid ↔ β and (ii) β ↔α. This system was reviewed by Murray (1981) (J. L. Murray, Liao, and Spear 1987) and investigated by different researchers, such as Farrar *et al.* (1966), Rudy and Windisch (1965), Chatterji *et al.* (Chatterji, Hepworth, and Hruska 1971), and Auffredic *et al.* (Auffredic, Etchessahar, and Debuigne 1982). Liquidus data for this system is not available, and solidus data was reported by Rudy (1969).

A limited amount of experimental thermochemical data for this system is available (Auffredic, Etchessahar, and Debuigne 1982) (Blacktop, Crangle, and Argent 1985) (Zee, Watters, and Davidson 1986). Thiedemann et al. (1999) reported mixing enthalpy

measurements of liquid Ti-Zr, Fe-Ti-Zr, and Fe-Ni-Zr alloys. Shin et al. (2006) have used first-principle calculations with SQS to determine the thermodynamic properties of binary hcp solution phases. Similar efforts have been made to obtain various thermodynamic data using First-principle calculations for the bcc Ti-Zr system (Catherine Colinet and Tedenac 2012) (Marker et al. 2018). The thermodynamic assessment of this system is given by Murray (1981), Hari Kumar *et al.* (Hari Kumar, Wollants, and Delacy 1994), and Turchanin et al.(Turchanin, Agraval, and Abdulov 2008), and Cui (2016). The work of Murray (1981) and Hari Kumar et al. (Hari Kumar, Wollants, and Delacy 1994) did not consider the mixing enthalpy of the liquid alloys (Thiedemann et al. 1999) in the Ti–Zr system. Later, Sridar et al. (Sridar, Kumar, and Kumar 2017) revised their assessment by considering the enthalpy of mixing the liquid phase.

Simultaneous optimization

The solidus data and the congruent melting temperature of (Rudy and Windisch 1965) were used in this work. For the congruent α/β transformation temperature, the work of Auffredic et al. (Auffredic, Etchessahar, and Debuigne 1982) was preferred. The selected data for α/β boundaries from Chatterji et al. (Chatterji, Hepworth, and Hruska 1971), Imgram et al. (Imgram, Williams, and Ogden 1962), and Hayes et al. (1955) were taken for optimization. Enthalpy of mixing data of Thiedemann et al.(1999) for the liquid phase, and SQS calculation data for the bcc phase were also considered for the parameter optimization.Table 4-3 gives the optimized parameters. It may be observed that a reasonably good description of the Gibbs energy for the bcc and hcp phases may be obtained by using parameters related to the first and second neighbor pair only. The calculated phase diagram is given in Figure 4-9 Solidus and liquidus boundaries are

compared with the experimental data in Figure 4-10, and a good agreement may be seen in Figure 4-11 shows the calculated and experimental α/β boundaries. Reasonable agreement between them may be observed. The invariant points in the phase diagram are presented in Table 4-4 along with earlier results. There is good agreement among all the results. Calculated enthalpy of mixing of the liquid phase at 2300 K (solid line) along with experimental data of Thiedemann et al.(1999) is shown in Figure 4-12. The calculated enthalpy of mixing data for the bcc phase has been compared to the data generated using first-principles calculations in Figure 4-13. Deviations from the first-principles calculations may be observed since more weightage is given to the experimental data while optimizing the parameters in this work.

Table 4-3 Optimized set of CECs used in assessing the Ti-Zr phase diagram.

Phase	Parameters (J/mol)
bcc_A2	$C_2^{\beta} = 183.0 - 0.1334 * T$ (I-neighbor pair)
	$C_3^{\beta} = 122 - 0.08893 * T$ (II-neighbor pair)
hcp_A3	$C_2^{\alpha} = -235 + 0.1213 * T$(I-neighbor pair)
	$C_3^{\alpha} = -235 + 0.1213 * T$ (II-neighbor pair)
Liquid	$L_0^{l} = -21000 + 8.427 * T$

Table 4-4 Invariant points in the Ti-Zr system

Invariants	Experimental data		Present work	
	T(K)	x_{Zr}	T(K)	x_{Zr}
Congruent (liquid ↔ bcc)	1810 (Rudy and Windisch 1965)	0.35	1811	0.356
Congruent (bcc↔ hcp)	875 (Auffredic, Etchessahar, and Debuigne 1982)	0.504	875	0.504

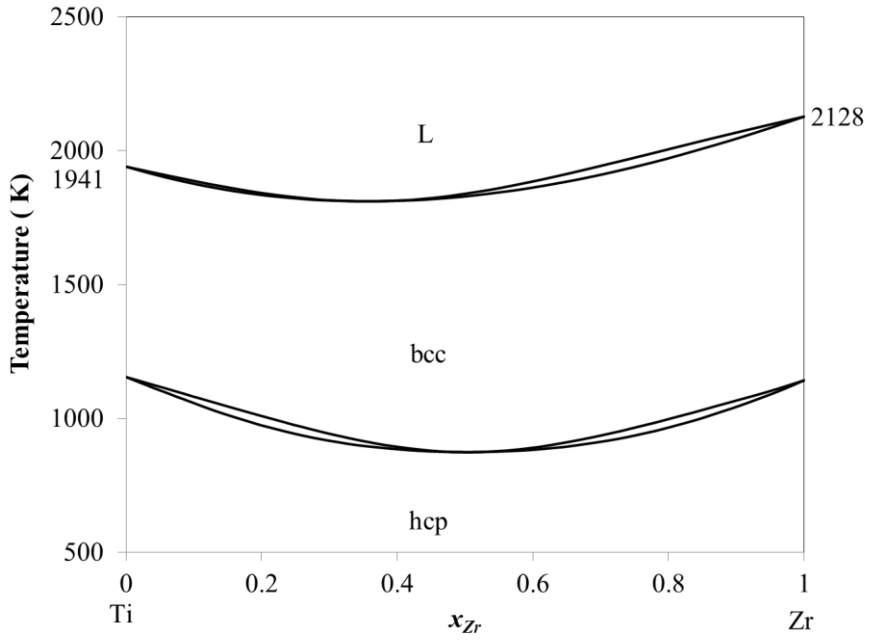

Figure 4-9 Calculated phase diagram and invariant points of the Ti-Zr system.

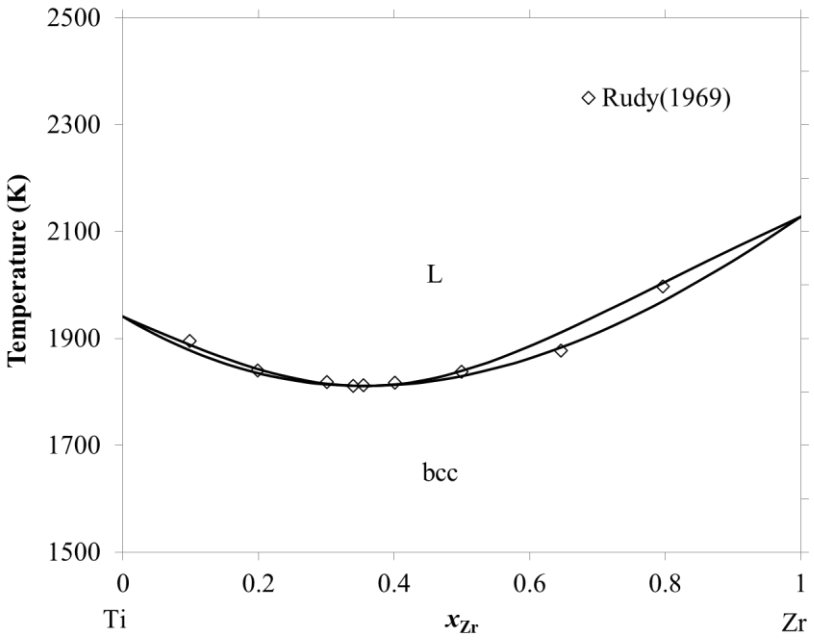

Figure 4-10 Calculated liquidus and solidus boundaries in the Ti-Zr system along with experimental data.

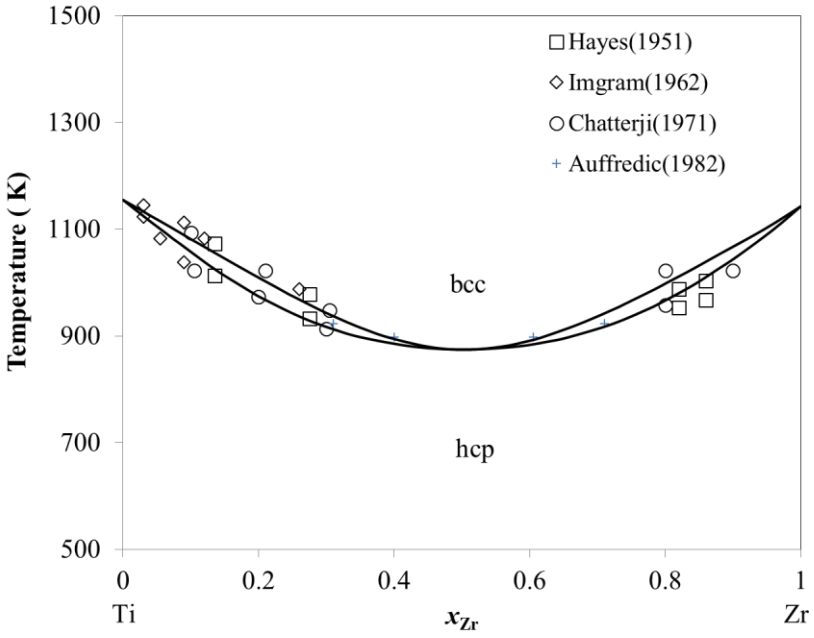

Figure 4-11 Calculated α/β boundaries and experimental data for Ti-Zr system.

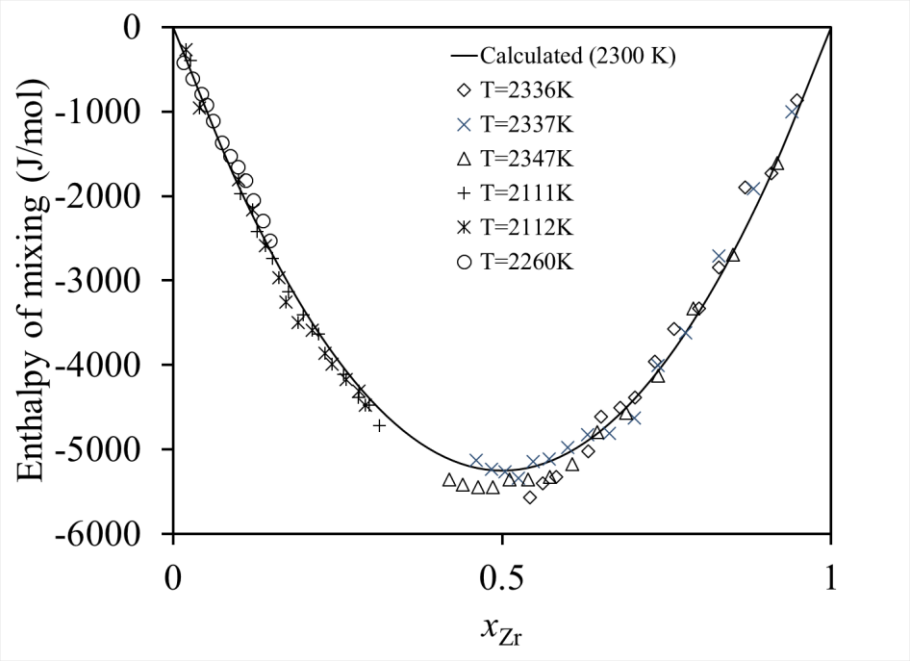

Figure 4-12 Calculated enthalpy of mixing for the liquid phase at 2300 K (solid line) and experimental data of Thiedemann et al. (Thiedemann et al. 1999) at various temperatures for Ti-Zr system.

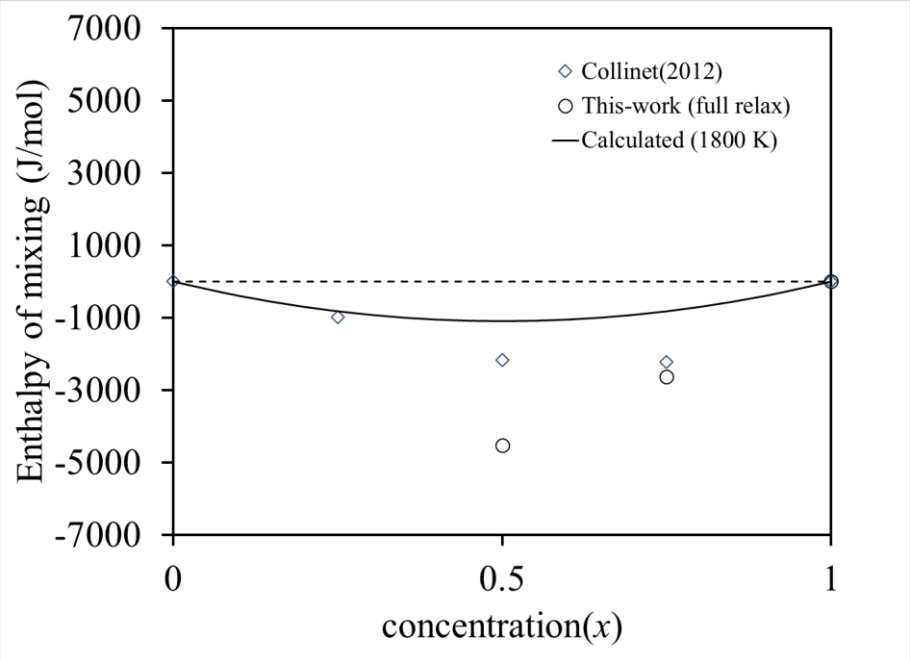

Figure 4-13 Calculated enthalpy of mixing for the bcc phase at 1800 K and first principle data for Ti-Zr system.

4.5 Nb-V system

Niobium and Vanadium are important alloying elements in steels and superalloys. It is finding newer applications in advanced materials like high entropy alloys and biomaterials in the recent past. Niobium helps to improve intergranular corrosion resistance in steel (Alonso-Falleiros and Wolynec 1998). The addition of Vanadium in Niobium has produced significant ultimate tensile strength, yield strength, and percentage elongation. Niobium and Vanadium are added to many alloys to increase their strength at high temperatures. Both elements are strong carbide formers and are hence useful for hardening and grain refining. Several High entropy alloys have recently been reported in which niobium addition plays a different role. Hence, the thermodynamic description of The Niobium-Vanadium binary system is essential for many important alloy systems.

The Nb-V system shows complete solid solubility and exhibits a congruent minimum. Recently, Gao *et al*. (2018) reported a miscibility gap in the system using isothermal treatment, diffusion couples experiment, and differential thermal analysis (DTA) technique. Rudy published the Nb-V phase diagram with the congruent minimum at 78.3. % V at 1860 °C and a single-phase bcc solid solution appears in the composition range (Rudy 1969). Baron et al. (Baron, Ivanova, and E.M. Savitskii 1960) observed the congruent minimum at 73.2 at.% at 1720 °C. Wilhelm (Wilhelm, Carlson, and Dickinson 1954) reported the congruent minimum at 77 % at 1810 °C. There are no experimental data available for the liquidus. Rudy's data is preferred as his observed melting points for V and Nb are close to currently accepted values for these metals (Smith and Carlson 1983).

Nb-V phase diagram computed by many researchers based on available experimental data. Molokanov et al. (V.V. Molokanov, D.B. Chernov 1977), Balakrishna and Mallik

(Balakrishna and Mallik 1979), and Smith *et al*. (Smith and Carlson 1983) calculated the Nb-V phase diagram and obtained a similar result as shown by Rudy (1969). Further, Kumar *et al*. (K. C. H. Kumar, Wollants, and Delaey 1994) studied the Nb-Ti-V phase diagram and re-optimized the Nb-V system. Recently, Gao et al. (2018) have reassessed this phase diagram based on their new experimental results. Different orders of Redlich-Kister polynomials (Redlich and Kister 1948) were used in all these works to model phases.

There was disagreement regarding a miscibility gap in the bcc phase at a lower temperature. Molokanov *et al*. (V.V. Molokanov, D.B. Chernov 1977) predicted a miscibility gap in the solid-state with composition at 50 at.% V at 380 °C. On the other hand, Smith *et al*. (1983) did not consider the miscibility gap to obtain the phase diagram. Gao et al. (2018) have reported the critical temperature of the miscibility gap at 50 at. % V at the temperature of 804 °C. The experimental finding of the miscibility gap by Gao *et al*. (2018) should settle this issue.

Ravi (2012) studied the Nb-V system using Density Functional Technique (DFT) and observed a miscibility gap at the low-temperature regime. They have reported the critical temperature of the miscibility gap at 677 °C and 977 °C using the cluster expansion with and without considering the constituent's strain and phonon contribution. Jiang et al. (2009) used SQS and found the enthalpy of mixing positive for this system. Available thermodynamic descriptions of the Nb-V system have not used calculated thermochemical data in the assessments.

Simultaneous optimization

As discussed earlier, there are two invariant reactions in the Nb-V system. For congruent melting, temperature and composition values observed by Rudy are widely accepted, and the same values have been used in this work. Similarly, the consolute point values of Gao

et al. (2018) have been accepted for this work. These two invariant reaction data points have been given more weightage during the optimization. The number of optimization parameters in the procedure described in the previous section gradually increased until all systematic deviations of the calculated values from the observed ones were eliminated. Efforts were made to keep the number of parameters minimum. The optimized parameters, along with those from previous assessments, are given inTable 4-5 . It is found that a reasonably good description of the Gibbs energy for the bcc phase may be obtained by using parameters related to the first and second neighbor pair only. The second neighbor pair CEC is fixed as 2/3rd of the first neighbor CEC since independent optimization of these parameters often leads to non-physical values. Temperature dependence of all the parameters was not needed to fit experimental data. Due to the different modeling approaches used, the model parameters for the bcc phase cannot be compared with those found earlier.

The calculated phase diagram is shown in Figure 4-14. A comparison with the numerous experimental data on the solidus and liquidus is given in Figure 4-15, and a reasonably good agreement may be seen. At lower temperatures, phase decomposition has been observed at 803.5 °C for 50 at. % V alloy. Figure 4-16 shows the calculated miscibility gap boundary and experimental information. Reasonable compliance between them may be observed. The invariant points in the phase diagram are presented in Table 4-6, along with earlier results. There is good agreement among all the results. Similarly, good agreement with thermodynamic data is obtained with optimized parameters, as shown in Figure 4-17.

Table 4-5 Optimized parameters for the Nb–V system

Phases	Parameters
Liquid (l)	$L_0^l = 9820$ J·mol^{-1}
bcc (β)	$C_1^\beta = -880$ J·mol^{-1} $C_2^\beta = -586.67$ J·mol^{-1} $C_3^\beta = 0.0$ J·mol^{-1} $C_4^\beta = 0.0$ J·mol^{-1}

*C_1^β, C_2^β, C_3^β and C_4^β Refer to the I-neighbor pair, II-neighbor pair, triangle, and tetrahedron CECs (Lele and Sarma 2009).

Table 4-6 Invariant points in the Nb-V system

Invariants	Rudy (Rudy 1969)		Kumar et al. (K. C. H. Kumar, Wollants, and Delaey 1994)		Gao et al. (J. Gao et al. 2018)		Present work	
	T(°C)	x_V	T(°C)	x_V	T(°C)	x_V	T(°C)	x_V
Congruent Minimum	1860	0.78	1858	0.783	1867	0.78	1858	0.78
Consolute Point	-	-	-	-	804	0.50	803.5	0.5

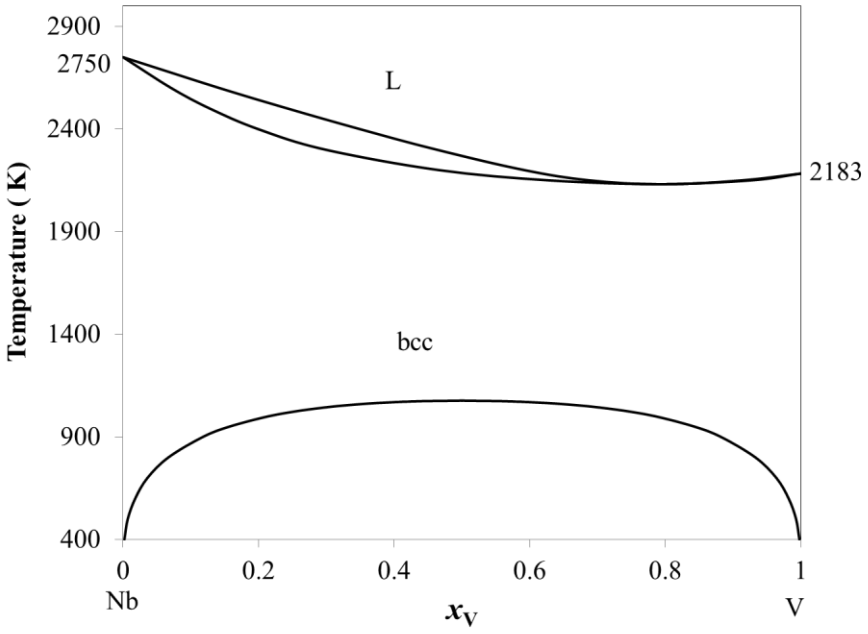

Figure 4-14 Calculated phase diagram and invariant points of Nb-V system.

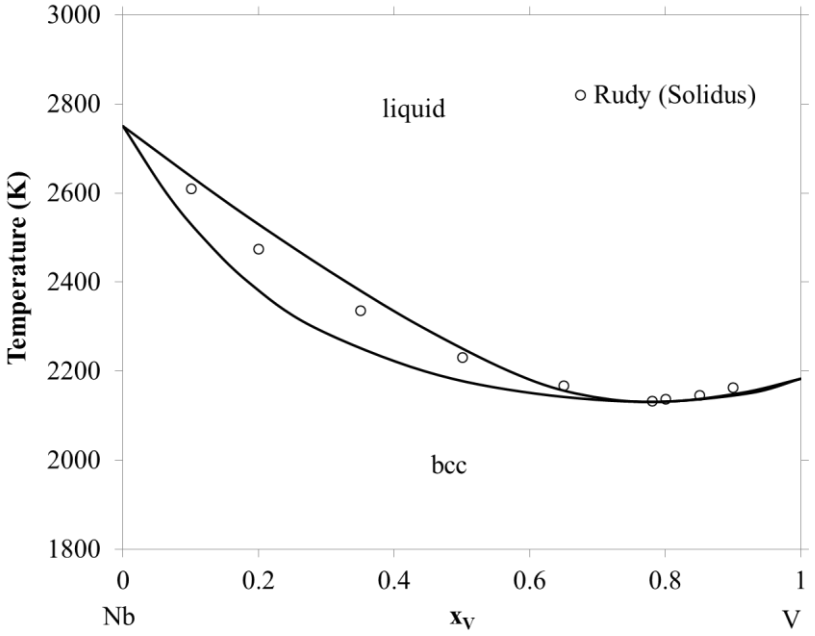

Figure 4-15 Calculated liquidus and solidus boundaries in the Nb-V system along with experimental data.

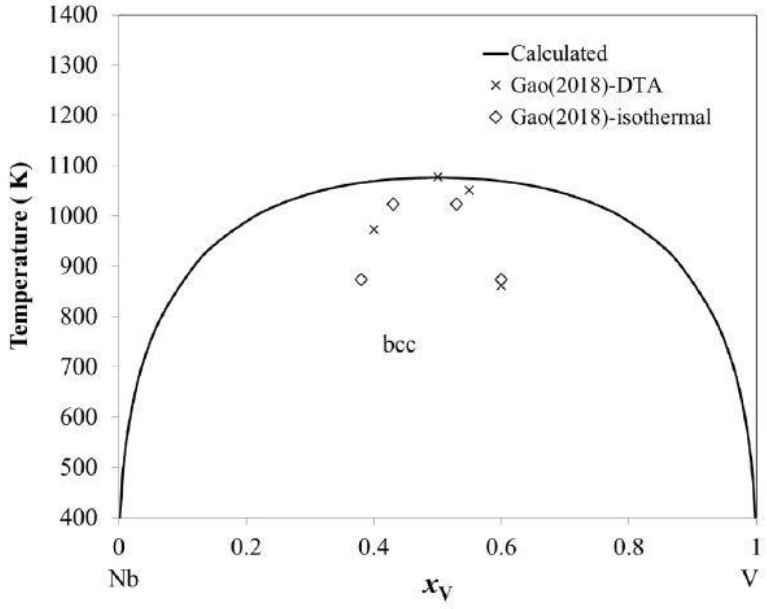

Figure 4-16 Calculated miscibility gap in the solid phase (solid line) and experimental data of Gao et al(2018) for Nb-V system.

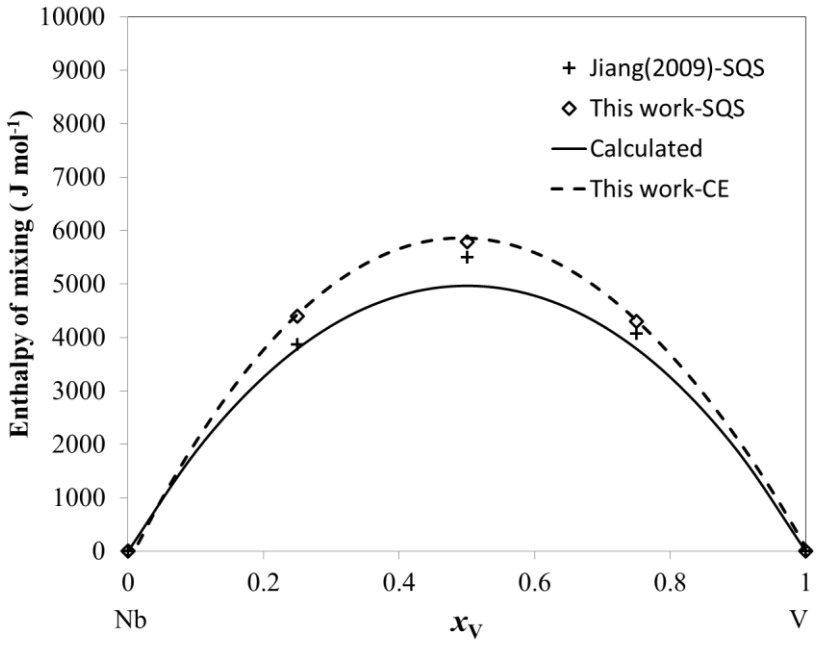

Figure 4-17 Calculated enthalpy of mixing of the solid phase at 2100 K (solid line) along with calculated data of Jiang et al.(2009) and in this work for Nb-V system.

4.6 Nb-Zr system

Niobium and zirconium are important alloying elements for superalloys and refractory alloys. Nb-Zr alloys exhibit excellent mechanical properties, superior corrosion resistance, low magnetic susceptibility, superconducting nature, and superior irradiation resistance. Due to their biocompatibility, they can also be used in biomedical applications such as knee and hip replacement for orthopedic surgeries (F. Y. Zhou et al. 2012). The Nb- Zr phase diagram is vital to understanding these alloys' structures and properties at various temperatures and compositions. Many efforts have been made to determine the phase diagram of this system, which was reviewed by Abriata et al. (1982) and Guillermet et al. (1991). In this system, there is complete miscibility in the liquid state, and the liquidus and solidus show a minimum point where the bcc_A2 (β) phase melts congruently. At high temperatures, the bcc_A2 phase covers the whole compositional range. In contrast, it exhibits a critical solution point at lower temperatures and a corresponding (βZr) + (βNb) miscibility gap. There is a monotectoid reaction (βZr) ↔ (αZr) + (βNb), which results in the coexistence of hcp_A3 (αZr) with (βNb). The solidus and the liquidus were measured by Rogers et al. (1955) and Lundin et al. (1960). Flewitt (1972) and Van Effenterre (1972) data are preferred for the miscibility gap. The solubility limits in the temperature range of interest are mainly based on the X-ray analysis of Flewitt et al. (1972) for the Nb-rich part and the experimental data (X-ray, resistivity, microscopical examination, and dilatometry) of Van Effenterre for the Zr-rich part (1972). No reliable experimental thermodynamic data is available for this system (Abriata and Bolcich 1982). Thermodynamic assessment of the Nb-Zr system has been done by Abriata et al. (1982), Guillermet et al. (1991), and Lafaye et al. (2019). These assessments describe the Gibbs energy of phases using the sublattice model within the Compound Energy Formalism Framework (CEF).

Cottura et al. (2018) have studied the solubility of the Zr-Nb system temperatures below 890 K using DFT. Barannikova et al. (2015) computed mixing enthalpies for hcp_A3, bcc_A2, and hypothetical fcc Zr-Nb alloys using ab initio methods. Interatomic potential for simulation of Zr-Nb system reported by Smirnova et al. (2017). Zhao et al. (2021) studied bcc_A2 ordered and disordered Nb-Zr systems using the first-principles method and reported positive formation energy in bcc_A2 Zr-Nb alloy. In lower Nb concentration (≤ 12.5 at%), the bcc_A2 Zr-Nb solid solution structure was unstable. Natarajan et al. (2020) have reported this system's cluster expansion (CE) study. However, available thermodynamic descriptions of the Nb-Zr system have not used calculated thermochemical data so far in the assessments.

Simultaneous optimization

As mentioned earlier, the phase diagram Nb-Zr system is characterized by three invariant reactions: congruent melting, critical point of miscibility gap, and monotectoid. For congruent melting, temperature and composition values observed by (Rogers and Atkins 1955) and (Lundin and Cox 1960) are in good agreement, and the same values have been used in this work. A dataset similar to Guillermet (1991) was used for liquidus and solidus boundaries. The consolute point and monotectoid temperature values of Flewitt et al. (1972) have been accepted for this work. These three invariant reaction data points have been given more weightage during the optimization. First, parameters for the bcc phase have been optimized using the miscibility gap and enthalpy of mixing data. With optimized bcc phase parameters, hcp phase parameters have been optimized using bcc-hcp phase equilibria data. Next, liquid phase parameters have been optimized using liquid and solidus data with optimized bcc phase parameters. Lastly, the entire parameter set is further refined with the complete dataset. The number of optimization parameters in the

procedure described in the previous section was gradually increased till all systematic deviations of the calculated values from the observed ones were eliminated. Efforts were made to keep the number of parameters minimum. The optimized parameters, along with those from previous assessments, are given in Table 4-7 . It is found that a reasonably good description of the Gibbs energy for the bcc phase may be obtained by using parameters related to the first, second neighbor pair, and triangle only. The second neighbor pair CEC is fixed as 2/3rd of the first neighbor CEC since independent optimization of these parameters often leads to non-physical values. Temperature dependence of some parameters was needed to fit experimental data. For the hcp phase, the minimal set consists of the first neighbor pair interactions (with the CECs corresponding to the in-plane and out-of-plane first neighbors being equal, $C_2^{\alpha} = C_3^{\alpha}$, that is, the interactions were assumed to be isotropic). Due to the different modeling approaches, the model parameters cannot be compared with earlier assessments.

The calculated phase diagram is shown in Figure 4-18. A comparison with the numerous experimental data on the solidus and liquidus is given in Figure 4-19, and a reasonably good agreement with the experimental data may be seen. At lower temperatures, phase decomposition has been observed. Figure 4-20 shows the calculated miscibility gap boundary and monotectoid reaction with experimental information. Reasonable compliance between them may be observed. The invariant points in the phase diagram are presented in Table 4-8 along with earlier results. There is good agreement among all the results.

Table 4-7 Optimized set of CECs used in assessing the Nb-Zr phase diagram.

Phase	Parameters (J/mol)
bcc_A2 phase	$C_2^{\beta} = -462.6 - 0.4152 * T$ (I-neighbor pair)
	$C_3^{\beta} = -308.4 - 0.2768 * T$ (II-neighbor pair)
	$C_4^{\beta} = 88.0$ (Triangle)
hcp_A3	$C_2^{\alpha} = -841.4$ (I-neighbor pair)
	$C_3^{\alpha} = -841.4$ (II-neighbor pair)
Liquid	L_0^l =-28060.0 + 21.72*T
	L_1^l =-24650 + 10*T

Table 4-8 Invariant points in the Nb-Zr system

Invariants	(Flewitt 1972)		(Abriata and Bolcich 1982)		(Fernandez Guillermet 1991)		Present work	
	T(K)	x_{Zr}	T(K)	x_{Zr}	T(K)	x_{Zr}	T(K)	x_{Zr}
Congruent Minimum	-	-	2013	0.783	2016	0.782	2017	0.755
Consolute Point	1253	0.40	1261	0.394	1250	0.413	1245	0.412
Three-Phase Equilibrium	893	0.10 (βNb) 0.85 (βZr) - (αZr)	893	0.09 (βNb) 0.815 (βZr) 0.994 (αZr)	893	0.079 (βNb) 0.813 (βZr) 0.993 (αZr)	895	0.074 (βNb) 0.797 (βZr) 0.986 (αZr)

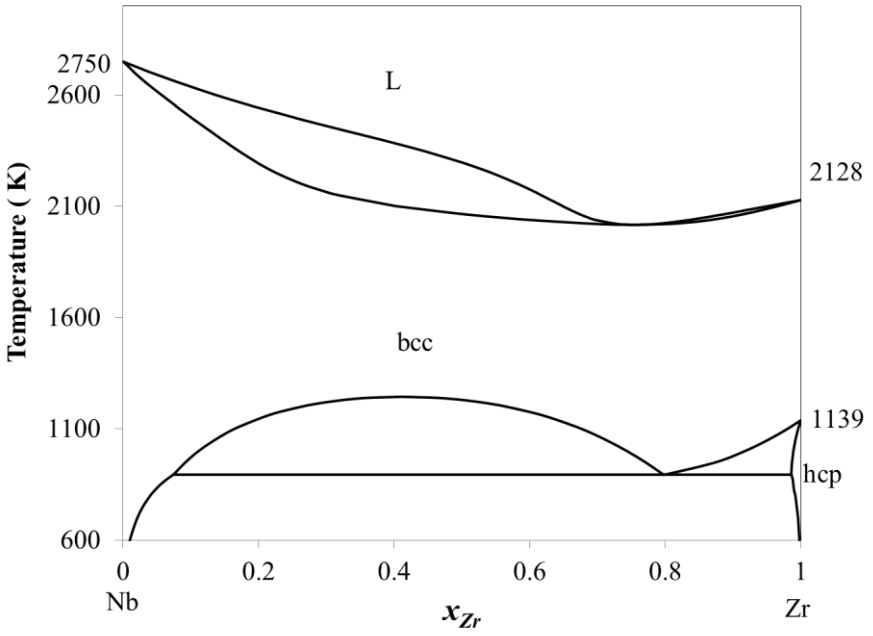

Figure 4-18 Calculated phase diagram and invariant points of the Nb-Zr system.

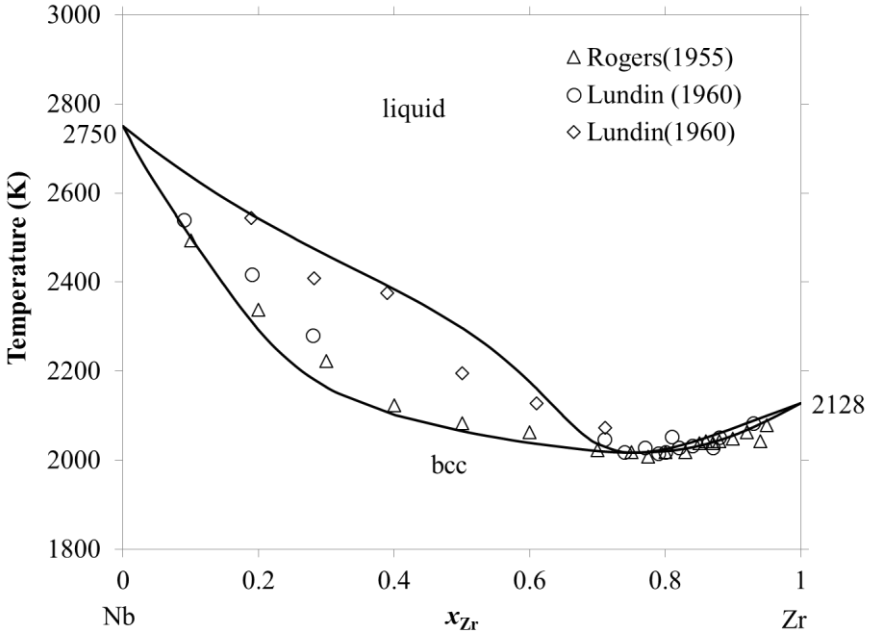

Figure 4-19 Calculated liquidus and solidus boundaries in the Nb-Zr system along with experimental data. The symbol (O) Ludin represents the solidus data whereas the symbol (◊) Ludin represents the liquids data.

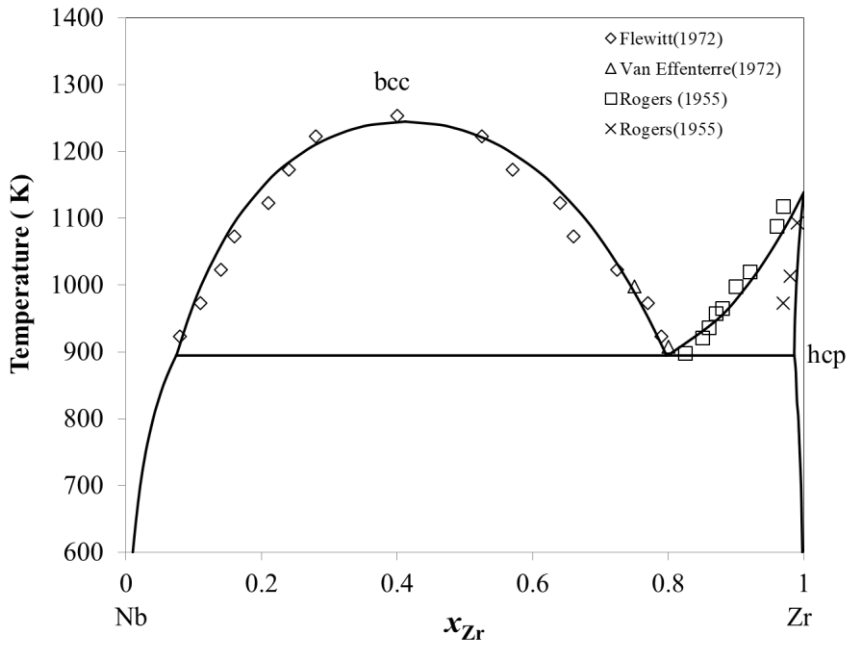

Figure 4-20 Calculated miscibility gap and monotectiod reaction in the solid phase (solid line) and experimental data of Nb-Zr system.

Enthalpies of mixing have been calculated at two temperatures, as shown in Figure 4-21. Calculated enthalpies of mixing are compared with those obtained from cluster expansion and SQS. Overall good agreement is found with cluster expansion results. However, SQS values show deviations from the calculated values near the Zr end.

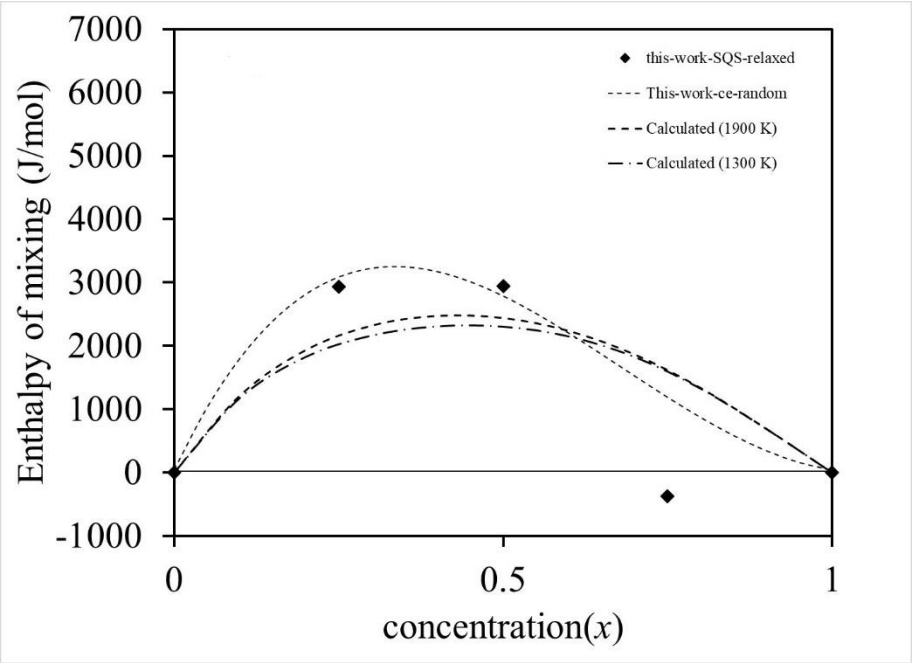

Figure 4-21 Calculated enthalpy of mixing of the solid phase at 1900 K (solid line) along with calculated data in this work for Nb-Zr system.

4.7 V-Zr system

The low-temperature superconducting behavior of β-V (5.2K) and **γ**-V_2Zr (8.5K) in the V-Zr phase diagram has been observed as promising outcomes for low-temperature applications. The grain boundaries and point defects formed during eutectic reactions are the main reason for the pinning of flux lines in low and high-magnitude fields. The critical current density was observed to be maximum in V rich phase ($x > 0$) in $V_{1-x}Zr_x$ system. The choice of composition and heat treatment conditions severely affect the critical current density of the alloy system. Revisiting the phase diagram of the Vanadium Zirconium system is very important. The physically sound model has been used in this study to reassess the phase diagram of the system. Wallbaum (1942) 1942 first reported the V-Zr system with the C14 ($MgZn_2$) type phase termed V_2Zr. Later in the year 1950, Anderson (1950) reported the solubility of a small amount of vanadium in zirconium. They reported the eutectic reaction between V_2Zr and Zr rich end. Pfeil (1952) 1952

further analyzed the phase diagram and reported the vanadium solubility to be 4.7 %. Later Rostoker and Yamamoto (Rostoker and Yamamoto 1954), in 1954, reported a eutectic reaction at 1360 ℃ and a peritectic reaction at 1740 ℃ with the V_2Zr phase. They reported 3% vanadium solubility in Zr. There was no report on Zr's rich side. Later in 1955, William (1955) reported the eutectic reaction at 1230 ℃ between V_2Zr and Zr end. The solubility of Vanadium in β Zr was reported to be 10%. Further V_2Zr decomposes into liquid and solid (containing 10% Zr in V). At 30% V, the eutectic reaction was reported. A eutectoid reaction was reported at 777 ℃ between V_2Zr and α Zr. The solubility limit between Zr and V was 5% at 600 ℃. The eutectic composition was at five wt% V. Massalski et al. (1990) reported in the year 1990 the 9% zirconium solubility in vanadium. The V_2Zr phase composition was reported at 47.2% Zr. A eutectic reaction was reported at 1265 ℃ and a peritectic reaction at 1300 ℃. The solubility of V in Zr was reported to be 8.9%. Zhao et al.(2012) 2012 assessed the phase diagram using the CALPHAD approach. The first principle approach was used to calculate the thermodynamic values. To predict the Gibbs energy of V_2Zr phases, the sub-lattice model was used. Strof et al.(2014) in 2013 extensively studied the Laves phase (V_2Zr) using ab-initio results. They reported a phase transformation from rhombohedral V_2Zr structure to cubic C15 Laves phase at about 115K. They reassessed the phase diagram and reported the model parameters.

Simultaneous optimization

The solidus data were taken from. For α/β boundaries, data were used. Enthalpy of mixing data given) was also considered to optimize the parameters. In the first step, parameters of the bcc_A2 phase were optimized with the help of the experimental enthalpy of mixing data. Next, parameters of the liquid phase were optimized using

solidus data, followed by the hcp_A3 phase using α/β boundaries data. Lastly, the parameters of all phases are refined further with the help of the entire dataset.

The optimized parameters are given in Table 4-9. Temperature dependence of all the parameters was not needed to fit experimental data. The calculated phase diagram is shown in Figure 4-22.

Table 4-9 Optimized set of CECs for the V-Zr phase diagram.

Phase	Parameters (J/mol)
bcc_A2 phase	$C_2^\beta = -1120 - 0.159 * T$ (I-neighbor pair)
	$C_3^\beta = -746.67 - 0.106 * T$ (II-neighbor pair)
	$C_4^\beta = 120.0$ (Triangle)

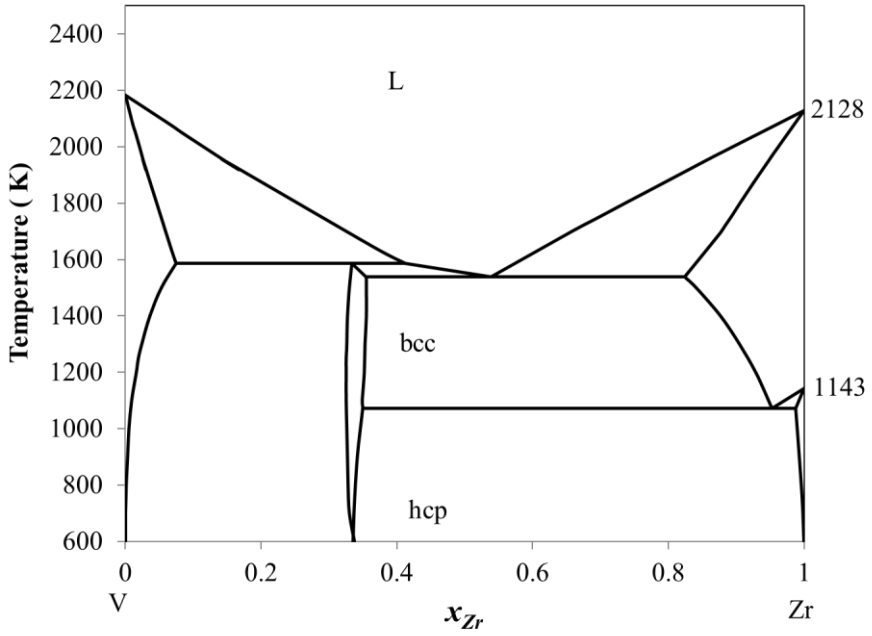

Figure 4-22 Calculated phase diagram of the V-Zr system.

4.8 Transformation of parameters from orthogonal basis to CV basis

A compilation of the binary CECs is given in Table 4-10. These CECs are in the orthogonal basis. These CECs are required to be transformed in the CV basis so that they remain invariant in the higher-order systems.

Table 4-10: The optimized CECs obtained from a binary assessment of the phase diagram.

System	1NN	2NN	Triangle	Tetrahedron
Nb-Ti	-390	-260	0	0
Nb-V	-880	-586.67	0	0
Nb-Zr	-462.6 -0.4152 T	-308.4 - 0.2768 T	88	0
Ti-V	-496 + 0.092 T	-330 + 0.06133 T	-12.142	0
Ti-Zr	183 - 0.1334 T	122 - 0.08893 T	0	0
V-Zr	-1120 - 0.159 T	-746.67 -0.106 T	120	0

In Appendix C, the following expressions for transforming CEC from the orthogonal to CV basis were derived for the binary bcc structure:

$$e21PQ = -16 \cdot C_2^{PQ} \quad 4.1$$

$$e22PQ = -12 \cdot C_3^{PQ}$$

$$e3PQ = -48 \cdot C_4^{PQ}$$

$$e4PQ = 96 \cdot C_5^{PQ}$$

CECs are transformed and included in the bcc Nb-Ti-V-Zr System description using the above expressions (Table 4-11).

4.9 Thermodynamic description of bcc Nb-Ti-V-Zr System

As mentioned earlier, CECs corresponding to the pure ternary and quaternary interactions are to be obtained from the cluster expansion of the ternary and quaternary systems. These results are given in sections 3.8 to 3.12. It was observed that these expansions resulted in CVs of the pair clusters only, and pure ternary and quaternary interactions were not included. It may be concluded that ternary and quaternary interactions are negligible for this system compared to binary interactions. Hence in the combined list of CECs (Table 4-11), only binary CECs, which are directly obtained from the assessments, were included, and CECs corresponding to pure ternary and quaternary interactions were kept zero.

Table 4-11 Thermodynamic descriptions of the bcc Nb-Ti-V-Zr system in the CF basis

CECs	values
e2NbTi1	6240
e2NbV1	14080
e2NbZr1	7401.6 + 6.6432 T
e2TiV1	7936 - 1.472 T
e2TiZr1	-2928 + 2.1344 T
e2VZr1	17920 + 2.544 T
e2NbTi2	3120
e2NbV2	7040
e2NbZr2	3700.8 + 3.3216 T
e2TiV2	3968 - 0.736 T
e2TiZr2	-1464 + 1.0672 T
e2VZr2	8960 + 1.272 T
e3NbTiV1	0
e3NbTiV2	0
e3NbTiV3	0
e3NbTiZr1	0
e3NbTiZr2	0
e3NbTiZr3	0
e3NbVZr1	0
e3NbVZr2	0
e3NbVZr3	0
e3TiVZr1	0

e3TiVZr2	0
e3TiVZr3	0
e3NbTi2	0
e3NbV2	0
e3NbZr2	-4224
e3TiV2	582.816
e3TiZr2	0
e3VZr2	-5760
e4NbTiVZr1	0
e4NbTiVZr2	0
e4NbTiVZr3	0
e4NbTiV1	0
e4NbTiV2	0
e4NbTiV3	0
e4NbTiZr1	0
e4NbTiZr2	0
e4NbTiZr3	0
e4NbVZr1	0
e4NbVZr2	0
e4NbVZr3	0
e4TiVZr1	0
e4TiVZr2	0
e4TiVZr3	0
e4NbTi2	0
e4NbV2	0
e4NbZr2	0
e4TiV2	0
e4TiZr2	0
e4VZr2	0

4.10 Conclusions

Thermodynamic assessments of all the six binary subsystems of the Nb-Ti-V-Zr system were done using all the available experimental data and FP-based thermochemical data. The Redlich-Kister formalism was used for the liquid phase, and the solid bcc and hcp phases were modeled by the phenomenological CE-CVM thermodynamic model. A consistent set of thermodynamic parameters has been arrived for describing the Gibbs energies of the solid and liquid solution phases. This leads to good agreement between

the calculated results and most of the experimental data in the literature. The CECs of the bcc phase for the binary systems and information of the higher order system were used to determine the thermodynamic description of the bcc Nb-Ti-V-Zr system.